Supporting Information

Novel Multilayer Nanostructured Materials for Recognition of Polycyclic Aromatic Sulfur Pollutants and Express Analysis of Fuel Quality and Environmental Health by Surface Enhanced Raman Spectroscopy

Olga E. Eremina [1], Alexander V. Sidorov [2], Tatyana N. Shekhovtsova [1], Eugene A. Goodilin [1,2,3,], and Irina A. Veselova [1]*

[1] Faculty of Chemistry, Moscow State University, Lenin Hills, 1-3, Moscow, 119991, Russia

[2] Faculty of Materials Science, Moscow State University, Lenin Hills, 1-73, Moscow, 119991, Russia

[3] Institute of General and Inorganic Chemistry, Leninskii prosp., 31, Moscow, 119071, Russia

AUTHOR INFORMATION

Corresponding Author

* Faculty of Materials Science, Moscow State University, Lenin Hills, Moscow,

119992, Russia. E-mail: goodilin@gmail.com; Fax: +7-(495) 939-09-98.

Charge transfer complexes (CTCs) in large concentrations are easily detected by UV-vis spectroscopy because their formation generally induced the appearance of a new absorption band usually reported as the Benesi-Hildebrand band. Dibenzothiophene (DBT) can act as π-type donor by the delocalized electrons of the aromatic rings (Fig. S1). 2,3-Dichloro-5,6-dicyanobenzoquinone (DDQ) has been used as π-acceptor due to its easy availability and its known capacity of forming CTCs.

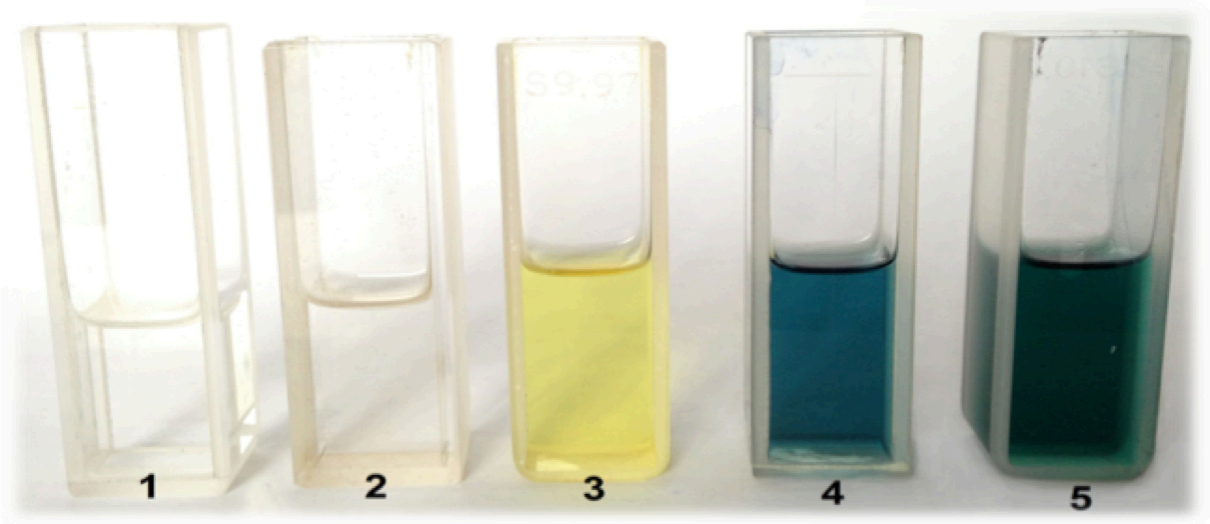

Figure S1. Visual formation of CTCs in $CHCl_3$: **1** – 5 mM DBT; **2** – 5 mM 4,6-DMDBT; **3** – 5 mM DDQ; **4** – 5 mM DBT:DDQ (1:1); **5** – 5 mM 4,6-DMDBT:DDQ (1:1).

Common π-acceptors (Fig. S2) have been tested to obtain the highest selective detection of one PASH against other aromatics. Among the investigated acceptor compounds, only DDQ and TCNQ formed CTCs with PASHs and oxidized form – DBTO.

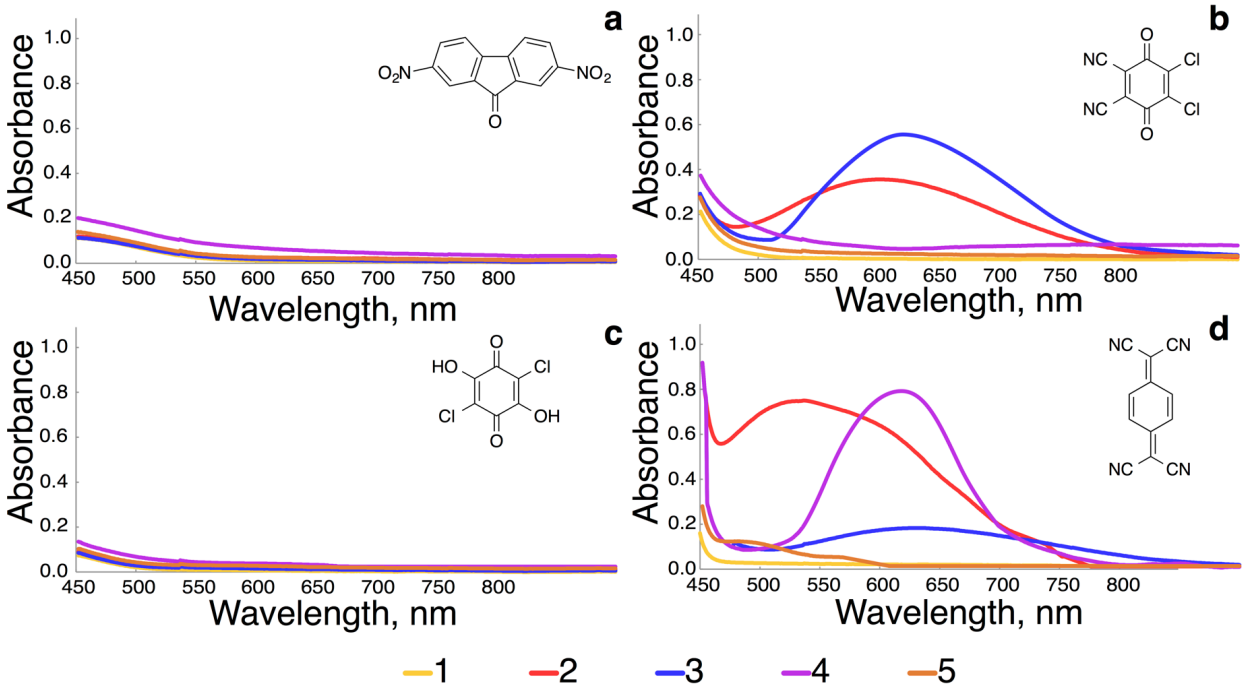

Figure S2. Absorbance spectra of different π-acceptors (1): 2,7-dinitro-9-fluorenone **(a)**, 2,3-dichloro-5,6-dicyano-*p*-benzoquinone **(b)**, 2,5-dichloro-3,6-dihydroxy-*p*-benzoquinone **(c)** and 7,7,8,8-tetracyanoquinodimethane **(d)**, and their CTCs with DBT (2), 4,6-DMDBT (3), DBTO (4), and $DBTO_2$ (5), correspondingly.

The calculation of the π-donor HOMO and the π-acceptor LUMO levels (Table S1) may allow a rough classification of their complexing abilities. As a first approach, neglecting geometrical or steric factors, we assume that the higher the level of π-donor HOMO, the lower π-acceptor LUMO and the smaller is the difference between them, therefore the stronger their association will be. The assumptions on complexes formation were confirmed by density functional theory (DFT) calculations of molecular orbitals of ether donors or acceptors. All the theoretical calculations were carried out using the Spartan`16 software. B3LYP method with 6-311+G** basis set was used in all the cases. This method provides both visualization of 3D-structures and quantum-chemical calculations. B3LYP stands for Becke, 3-parameter, Lee-Yang-Parr. B3LYP

is a hybrid functional method (approximation to the exchange-correlation energy functional in DFT that incorporate a portion of exact exchange from Hartree-Fock theory with exchange and correlations from other sources) is commonly used versions.

Table S1. Difference in E_{LUMO} of π-acceptor (*A*) and E_{HOMO} of π-donor (*D*)

$E^{A}_{LUMO} - E^{D}_{HOMO}$, eV	DBT	4,6-DMDBT	DBTO
DDQ	0.72	0.59	1.73
TCNQ	0.96	0.83	1.87

Following the method of Foster-Hammick-Wardley, this phenomenon allows the calculation of the association constant (and hence the Gibbs free energy) characterizing the new complexes[S1]. In order to compare the stability of the complexes of the studied sulfur compounds with DDQ/TCNQ in chloroform the equilibrium process of their formation can be schematically represented as follows:

$$D + A \overset{K_f}{\leftrightarrow} DA \quad (1)$$

where *D* – donor, *A* – acceptor and *DA* – formed CTC.

By introducing the approximation that $[A]_0 >> [D]_0$, and considering that the optical path length (*l*) is 1 cm (5), the expression for the stability constant of the complex: $K_f = \frac{[DA]}{[D]\cdot[A]}$ can be transformed into equation suitable for K_f calculation from experimental data using the formula:

$$\left.\begin{array}{l} K_f = \dfrac{[DA]}{\{[D]_0 - [DA]\} \cdot \{[A]_0 - [DA]\}} \quad (2) \\ \{[D]_0 - [DA]\} \approx [A]_0 \quad (3) \\ Abs = \varepsilon \cdot l \cdot [DA] \quad (4) \\ l = 1\ cm \quad (5) \end{array}\right\} \Rightarrow \frac{[D]_0}{Abs} = \left(\frac{1}{[A]_0}\right) \cdot \left(\frac{1}{\varepsilon \cdot K_f}\right) + \frac{1}{\varepsilon} \quad (6)$$

The association constant K_f from (2) for complex formation was calculated by the linearization of the Benesi-Hildebrand equation in the coordinates $x = \frac{1}{[A]_0}$; $y = \frac{[D]_0}{Abs}$.

The molar absorption coefficient was found as the inverse value of the segment (9), extrapolated intercept obtained a graph on the *Y*-axis. The constant was calculated from the value of the line slope (10):

$$\begin{cases} \dfrac{[D]_0}{Abs} = a \cdot \dfrac{1}{[A]_0} + b \quad (7) \\ \dfrac{[D]_0}{Abs} = \left(\dfrac{1}{\varepsilon \cdot K_f}\right) \cdot \left(\dfrac{1}{[A]_0}\right) + \dfrac{1}{\varepsilon} \quad (8) \end{cases} \Rightarrow \begin{cases} \varepsilon = \dfrac{1}{b} \quad (9) \\ K_f = \dfrac{b}{a} \quad (10) \end{cases}.$$

The number of experimental values of *Abs* obtained by varying the total concentration of acceptors: DDQ or TCNQ ($[A]_0 = var$) with the fixed total concentration of π-donors: DBT, 4,6-DMDBT or DBTO ($[D]_0 = const$). To comply with the condition $[A]_0 >> [D]_0$, the concentration ratio $[D]_0 : [A]_0$ was varied from 1:75 to 1:100. Extrapolation of the experimental line which points are very far from the y-axis, does not give a very accurate value for free term b of the linear equation $y = ax + b$ and, therefore, makes a significant error in the calculation of the thermodynamic quantities (K_f and ΔG) given in Tables S2, S3. However, to assess the interaction of π-donor/π-acceptor complexes and comparison of stability between them this way is quite applicable.

Table S2. Association constant (K_f) values characterizing the new complexes (n = 7, P = 0.95)

K_f, M^{-1}	DBT	4,6-DMDBT	DBTO
DDQ	21 ± 1	143 ± 8	4.0 ± 0.3
TCNQ	7.2 ± 0.9	19.6 ± 0.9	77.8 ± 4.3

Firstly, it is possible to make a conclusion from K_f values that the complex with DDQ is the most stable for DBT, also for 4,6-DMDBT, and TCNQ is the case for DBTO. Secondly, the influence of oxidized forms on determination of 4,6-DMDBT and DBT with DDQ would not be insignificant. A quite interesting observation is that the stability constants calculated from the experimental data for the DDQ complexes correlated fully with the difference in the theoretical energy levels obtained for π-acceptor LUMO and π-donor HOMO. It was established that the stability of complexes with DDQ in chloroform increases for π-donors: DBTO → DBT → 4,6-DMDBT antisymbatic with increasing ($E_A - E_D$) (Table S1). However, the situation is quite different for TCNQ complexes: despite the relatively high value of $E_{TCNQ} - E_{DBTO} = 5.98$ eV the complex was the most stable in the series. To explain this fact, the presence of the oxygen atom in the structure of DBTO can be considered and related geometric redistribution of the electron density of the HOMO, which is as important as the energy difference between the LUMO and the HOMO (Fig. 1).

Table S3. Gibbs free energies ($-\Delta G$) values characterizing the new complexes (n = 7, P = 0.95)

$-\Delta G$, kJ/mol	DBT	4,6-DMDBT	DBTO
DDQ	7.6 ± 0.4	12.3 ± 0.7	3.4 ± 0.5
TCNQ	4.9 ± 0.6	7.4 ± 0.3	10.8 ± 0.6

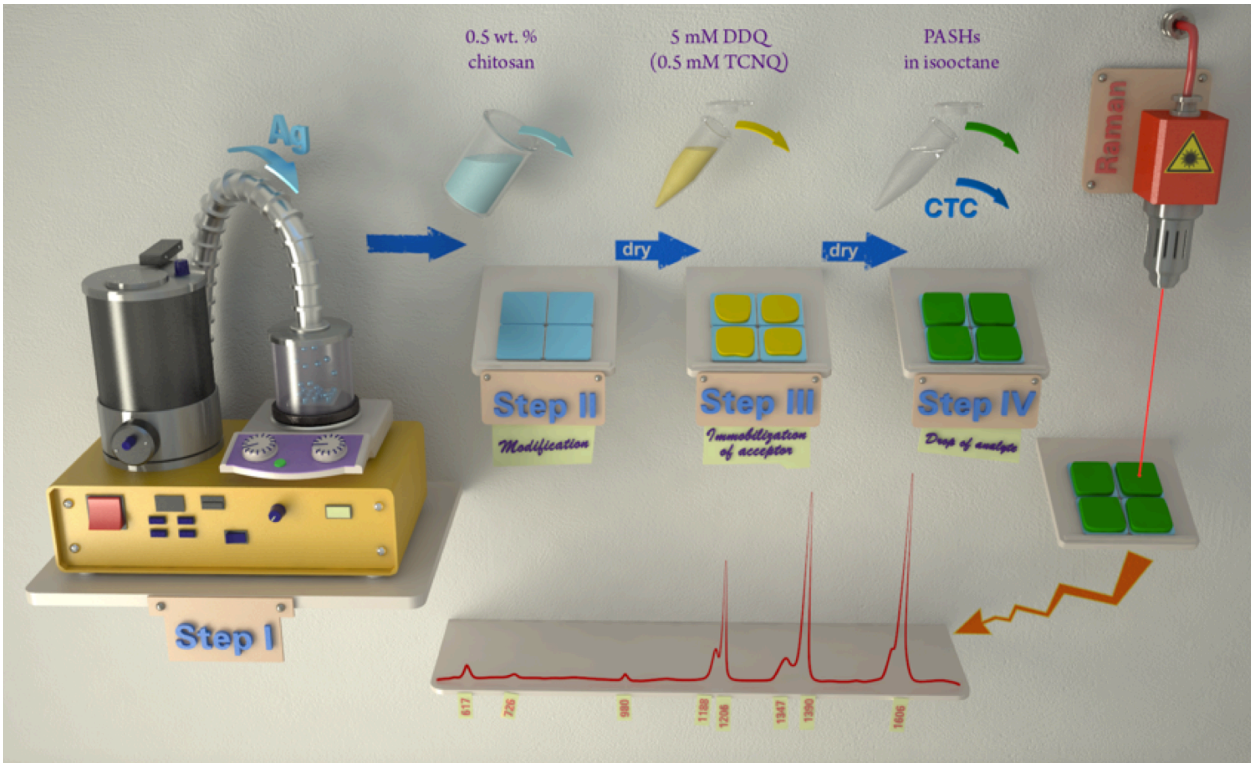

Figure S4. The scheme of the process: from creating the sensor during ASP-procedure to analysis with resonance SERS spectroscopy with the formation of charge transfer complex on the sensor surface.

SERS experiments were carried out on planar optical materials based on nanostructured silver sensor. Silver ring structures caused by the known "coffee ring" effect are formed at moderate temperatures of 200 – 250 °C due to deposition of the mist droplets onto a preheated substrate (Fig. S4, Step I). The coatings consist of overlapping silver rings of a complex morphology originated from decomposition of micrometer-sized droplets of ultrasonic mist of silver (I) solution. This resembles a rain making rings on a flat dusty surface, hence, we call it Ultrasonic Silver Rain (USSR). Usually, silver deposition gives intersecting circles of 30 – 100 μm in diameter. The silver surface was coated with a thin layer of microporous optically transparent chitosan gel (Fig. S4, Step II) and DDQ or TCNQ was immobilized on the surface (Fig. S4,

Step III). After that only a drop of a sample should be put (Fig. S4, Step IV) and a SERS spectrum registered (Fig. S4, Step V). Resonant SERS spectra were registered using a red laser (λ_{ex} 633 nm) since, according to spectrophotometry data, it should resonantly agitate the obtained CTCs (λ_{max} 600 – 650 nm).

The obtained nanostructured silver substrates were characterized by scanning electron microscope (SEM) using Carl Zeiss NVision 40, by transmission electron microscopy (TEM) and electron diffraction (ED) (Fig. S5) using LEO912AB OMEGA (Carl Zeiss) at 100 kV accelerating voltage. A study of the obtained samples jn a transmission electron microscope (Fig. S5, left) showed that silver nanoparticles have a wide size distribution (5 – 70 nm), what is typical for long processes of nucleation and growth. Electron diffraction image shows the presence of silver assembly metallic silver (Fig. S5, right).

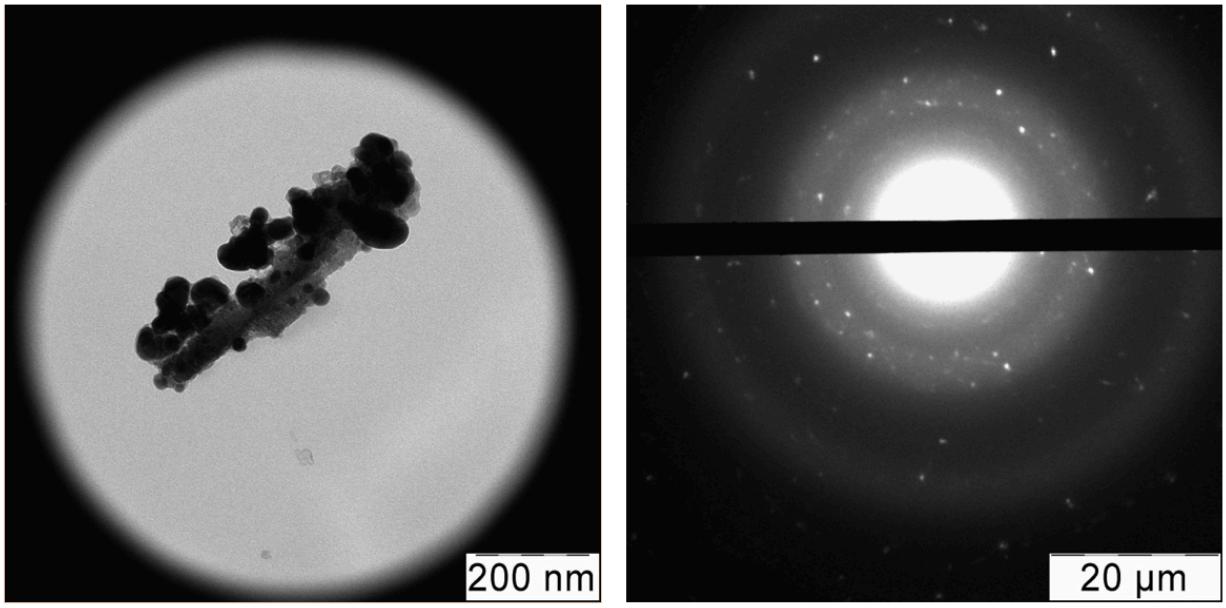

Figure S5. Typical transmission electron microscopy (TEM) images (left) and electron diffraction (ED) of fragments (right) of nanostructured of silver substrates.

The obtained SERS-active silver structures were tested on the model analyte – the dye Rhodamine 6G with concentration 1×10^{-8} M to optimize the parameters of silver surface preparation (Fig. S6).

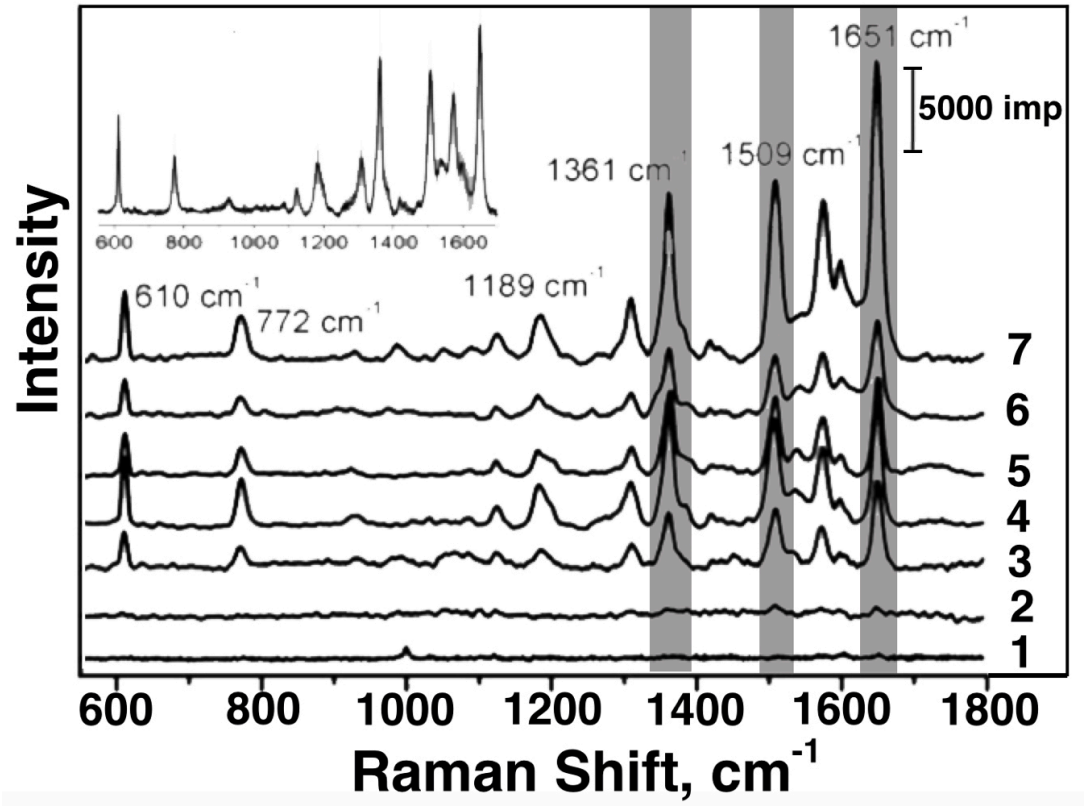

Figure S6. SERS spectra of a model dye – Rhodamine 6G (1×10^{-8} M) on the nanostructured silver surfaces obtained by ASP-procedure (chemical way) with the deposition time 30 s (1), 90 s (2), 5 min (3), 10 min (4), 20 min (5), 25 min (6), 15 min (7), the inset shows spectra (7) with standard deviation in grey. The SERS spectra are typical for the freshly prepared silver substrates and the substrates obtained 12 months ago. The inset represents averaged SERS spectra measured in 5 – 10 different points on the surface of the substrate (the area marked in gray on the spectrum corresponds to the standard deviation of the spectral intensities). All the SERS spectra are measured using a 514 nm laser and power neutral density filter (10%), 20× objective lens and 10 s of acquisition time.

The indicator SERS-systems for determining DBT and DBTO were chosen based on previous spectrophotometric studies. In order to optimize the sample preparation we considered different sequences of applying complex DBT:DDQ or DBTO:TCNQ on a metal substrate (Fig. S7, Table S4).

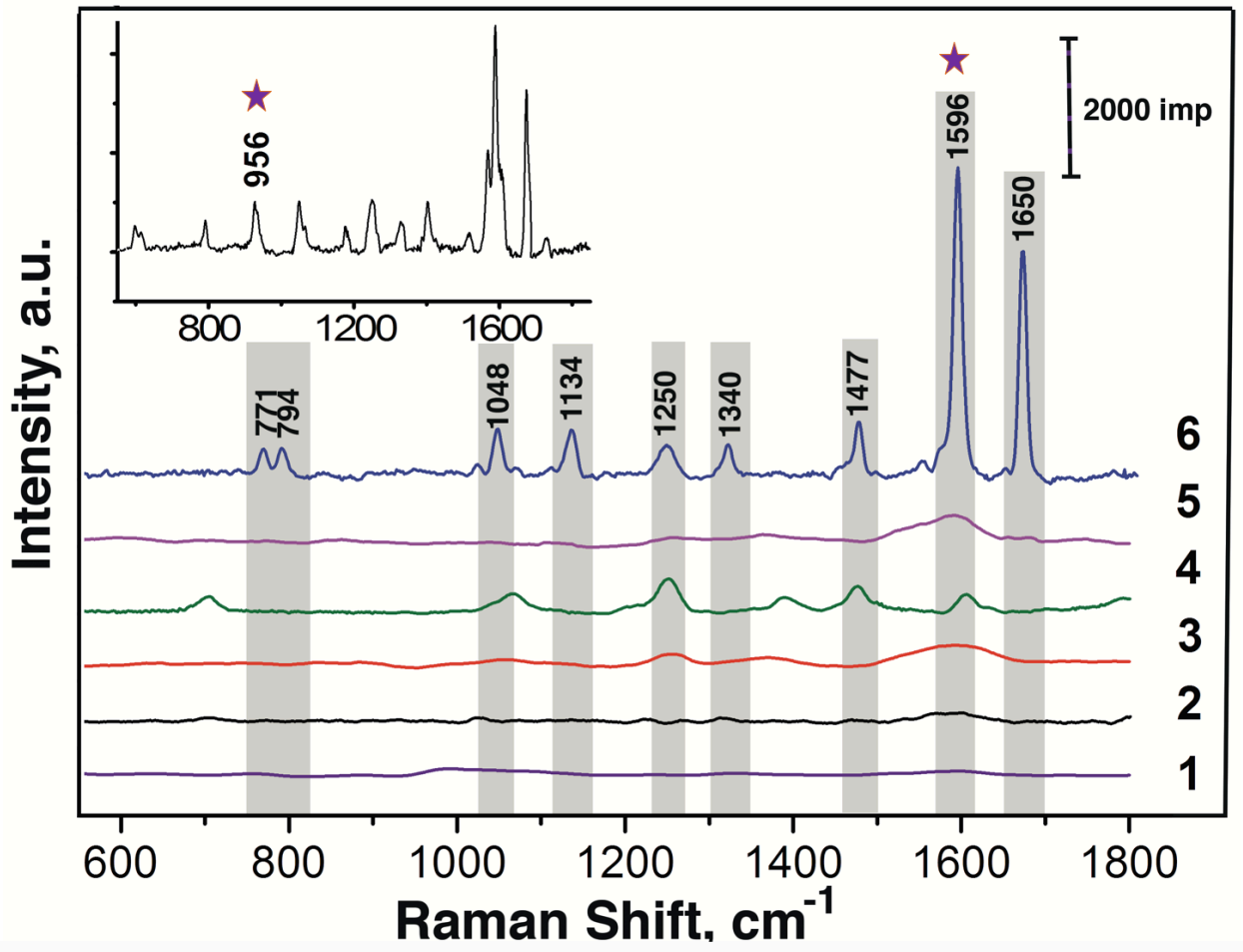

Figure S7. RS spectra of DBT (1), DDQ (3), DBT:DDQ complex 1:1 (5), and SERS spectra on nanostructured silver surface of DBT (2), DDQ (4), and DBT:DDQ complex 1:1 (6). The concentrations of all analytes – 1×10^{-4} M. Instrumental parameters: 10%; 633 nm; 10 s.

Table S4. Methods of application of the complex DBT:DDQ on a metal substrate

	The sequence of applying the complex DBT:DDQ a metal substrate
Method 1	1. Silver substrate was modified with chitosan 0.5 wt %
	2. Complex were deposited on the substrate surface after had been obtained in solution
Method 2 (4)	1. The substrate silver surface was coated by DDQ (TCNQ) solution and dried
	2. On the same surface was applied a solution of the analyte – DBT (DBTO)
Method 3	1. Silver substrate was modified with chitosan 0.5 wt %
	2. The substrate surface was coated by DDQ solution and dried
	3. On the same surface was applied a solution of DBT

The concentration of the applied DDQ solution was verified, and the concentration of DBT was constant to find the optimal concentration of the π-acceptor immobilized on the substrate. The characteristic frequency of 1596 cm^{-1} (aromatic moiety DBT signal) has been selected as an analytical signal (Fig. S8).

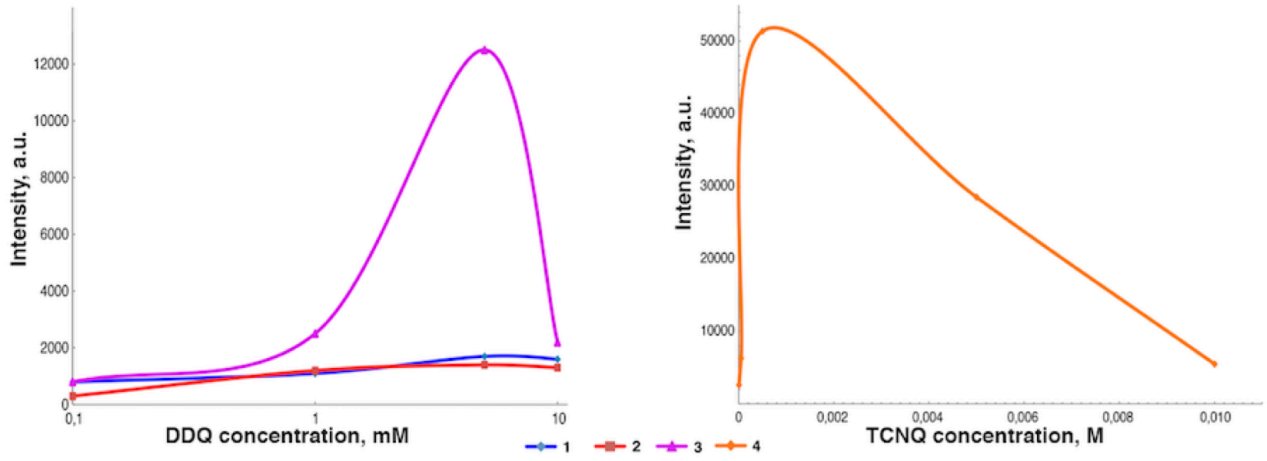

Figure S8. The dependence of SERS intensity for 0.1 mM DBT (1596 – 1598 cm^{-1}) on DDQ concentration for different sequence of CTC applying: (1) method 1, (2) and (4) method 2 and 4, (3) method 3.

The results obtained when applying the proposed technique were confirmed by a standard GC-MS analysis (Fig. S9) for DBT determination, but the selectivity across different oxidized forms of DBT can be achieved only using an additional column.

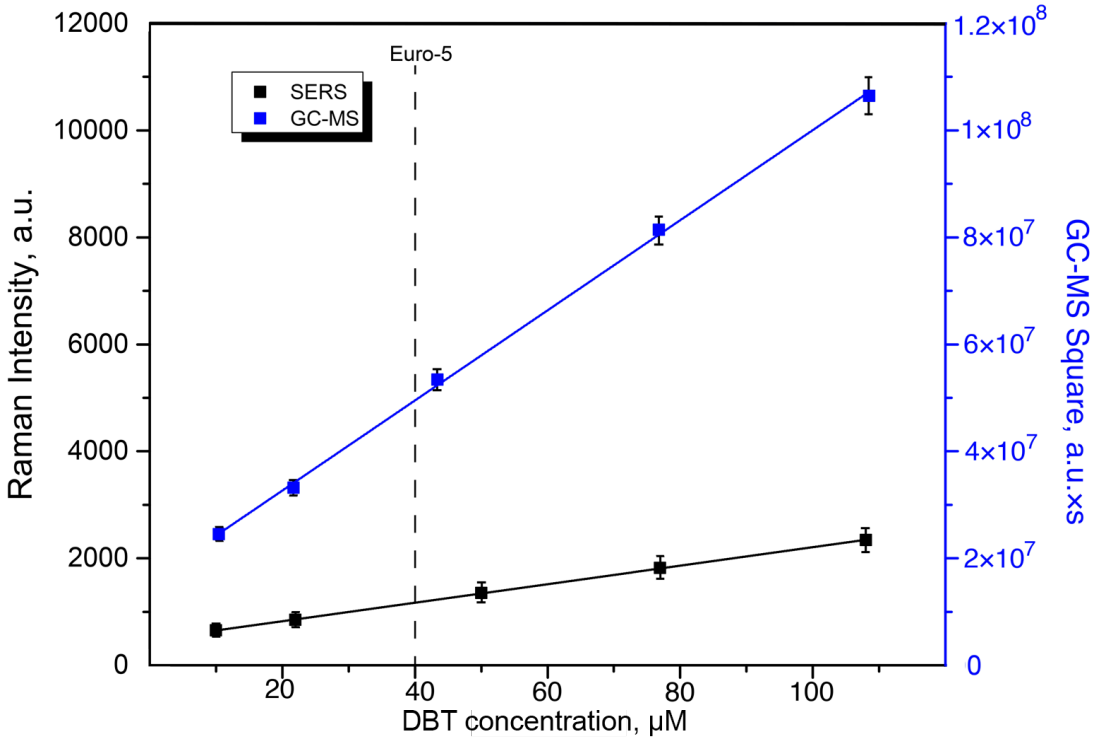

Figure S9. SERS and GC-MS analyzes of a petroleum sample (with 95 octane rating and "Euro-5" quality) with different quantity of added DBT.

Reproducibility of the SERS spectra for detecting charge transfer complex of DBT (Fig. S10) and DBT in the presence of oxidized forms (Fig. S10, S11) with DDQ were tested with standard deviation corridors (n = 10; P = 0.95).

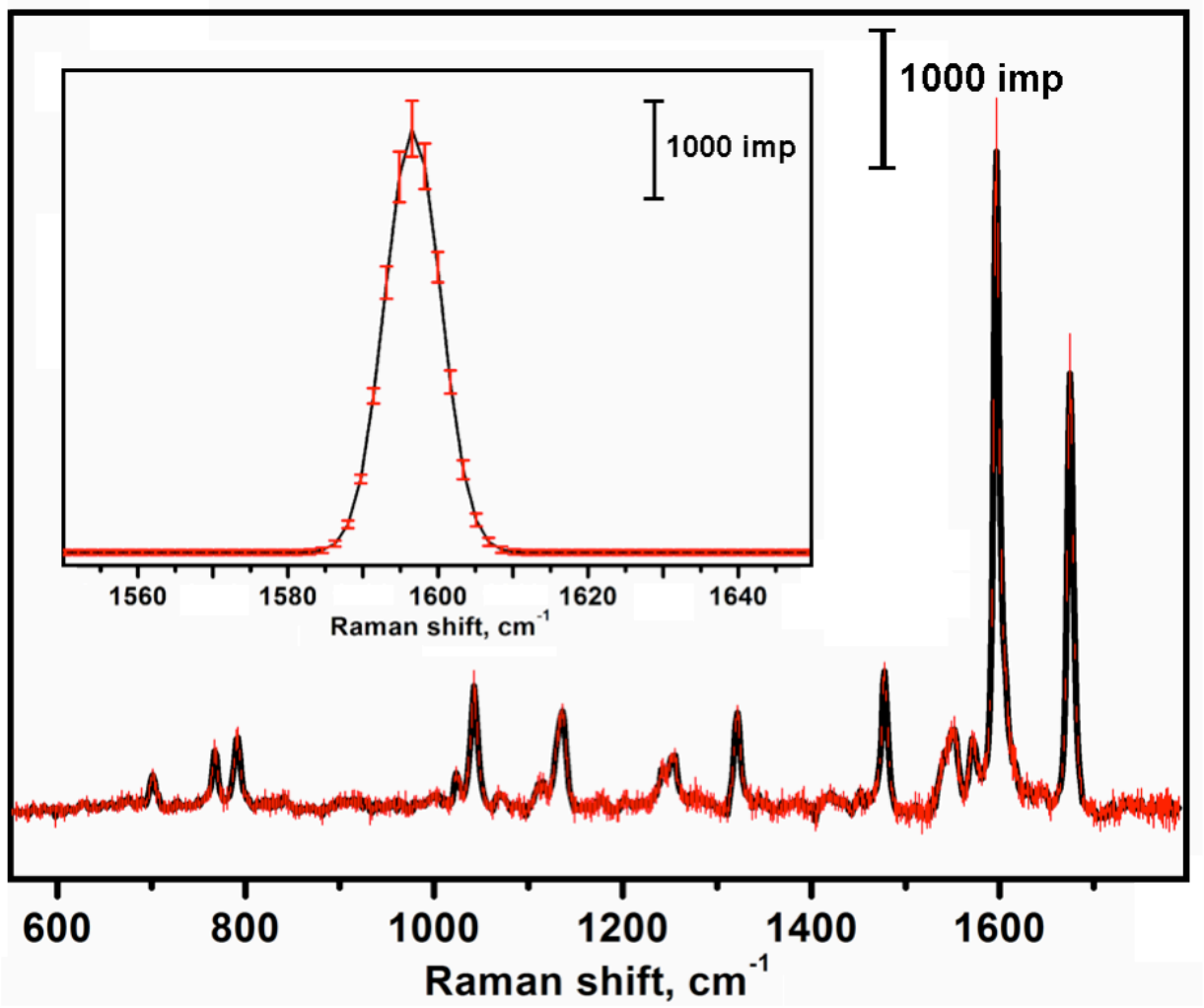

Figure S10. Reproducibility of SERS spectra for charge transfer complex of DBT (0.1 mM) and DDQ (5 mM) with standard deviation corridors (n = 10; P = 0.95). The inset shows Gauss description of the characteristic peak 1596 cm^{-1}.

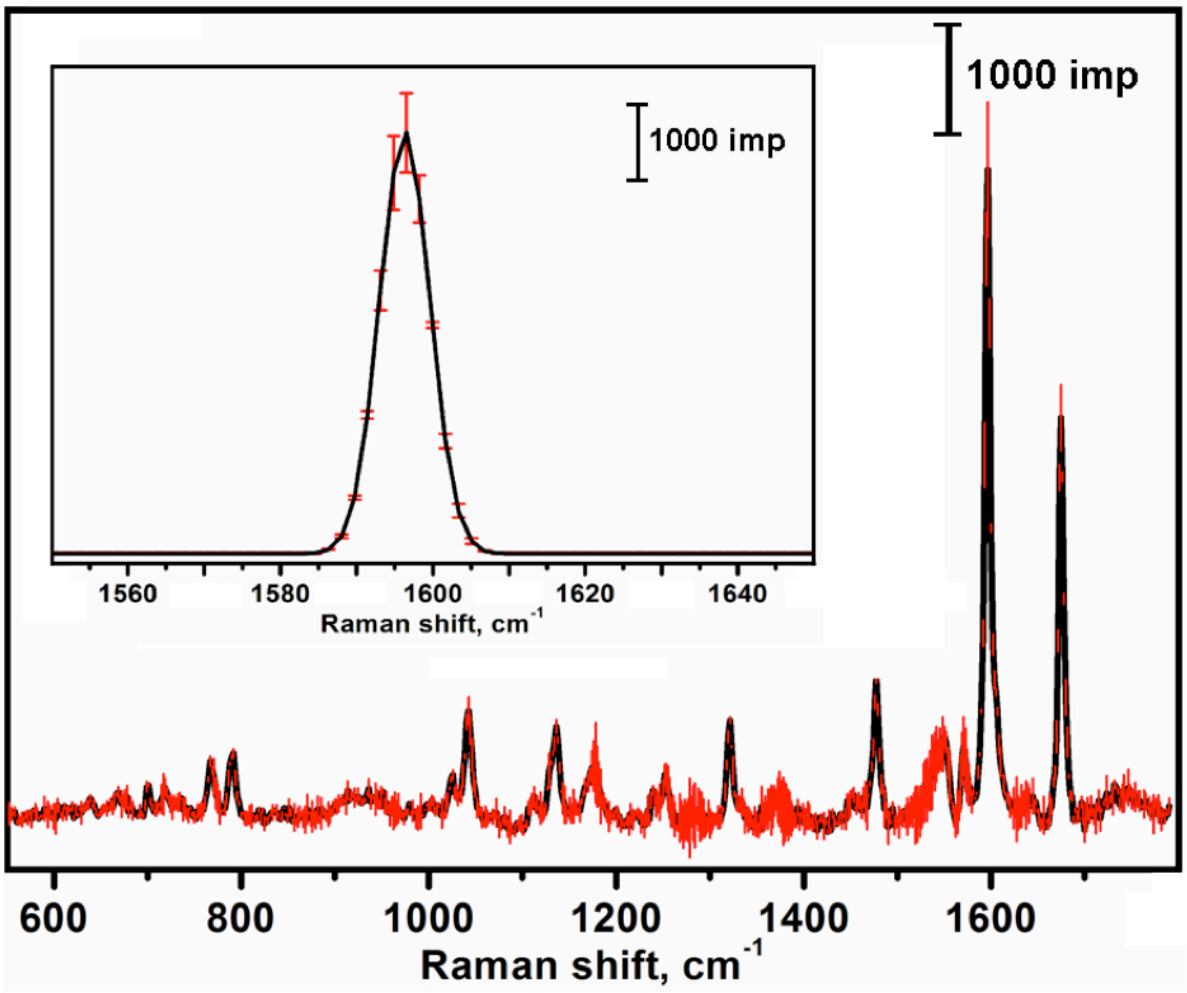

Figure S11. Reproducibility of SERS spectra for charge transfer complex of DBT (0.1 mM) and DDQ (5 mM) in the presence of DBTO (0.2 mM) with standard deviation corridors (n = 10; P = 0.95). The inset shows Gauss description of the characteristic peak 1596 cm^{-1}.

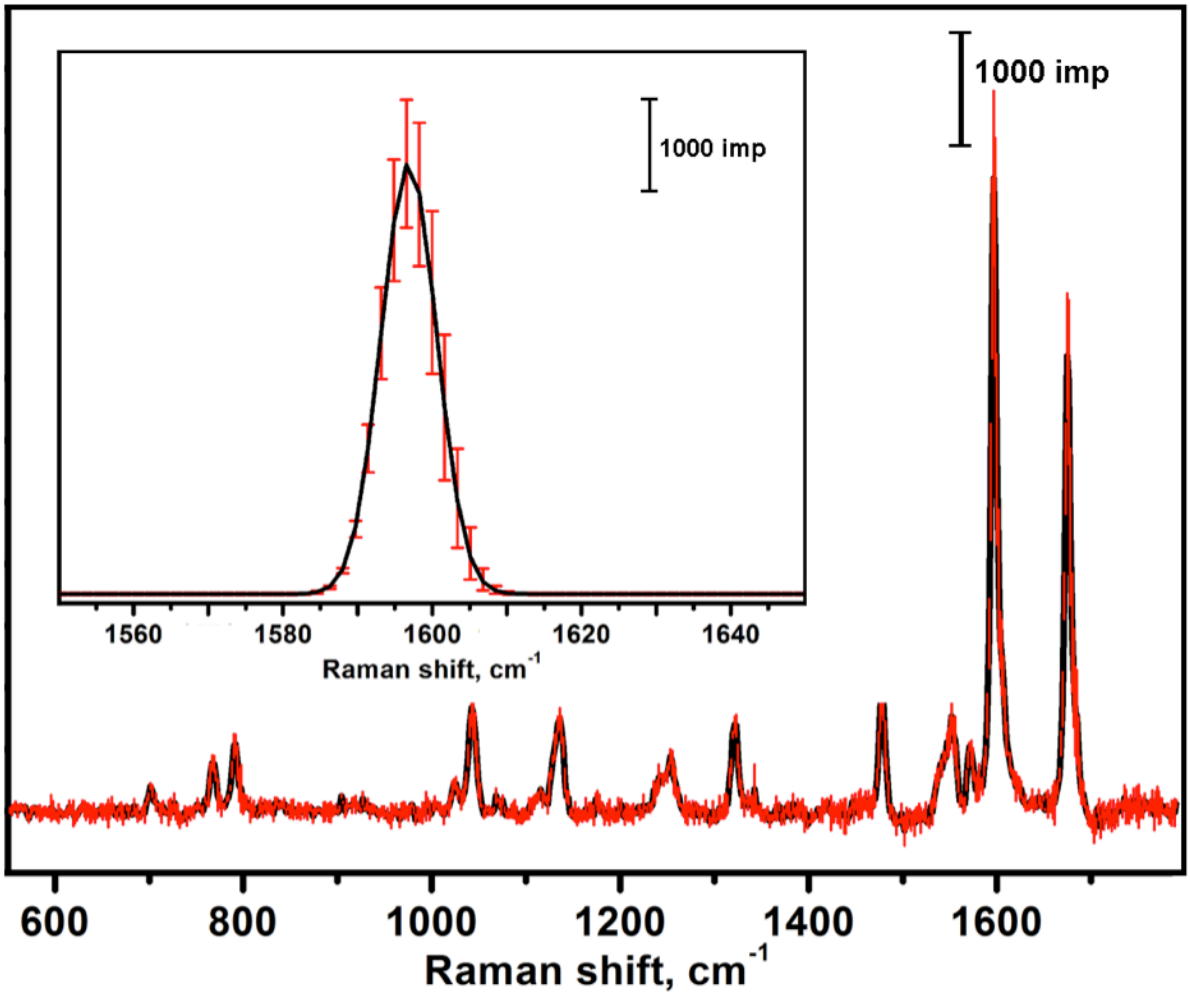

Figure S12. Reproducibility of SERS spectra for charge transfer complex of DBT (0.1 mM) and DDQ (5 mM) in the presence of $DBTO_2$ (0.2 mM) with standard deviation corridors (n = 10; P = 0.95). The inset shows Gauss description of the characteristic peak 1596 cm^{-1}.

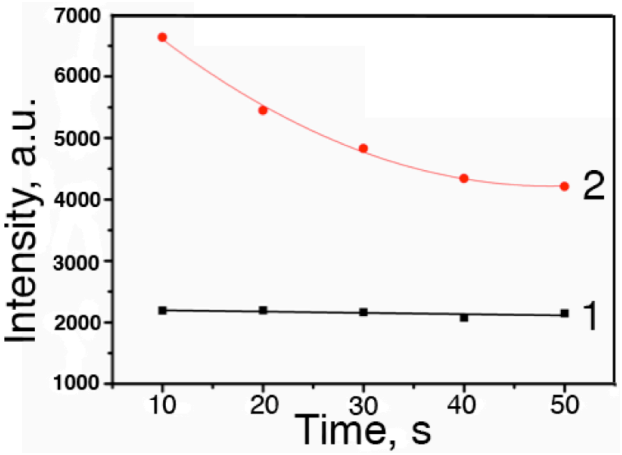

Figure S13. Photodegradation of charge transfer complex of DBT (0.1 mM) and DDQ (5 mM) in one spot of nanostructured silver surface with red laser (633 nm) with power densities 1% (1) and 10% (2).

Table S5. Analysis of the main quality of petroleum products in the presence of markers of the main conversion product – $DBTO_2$ – (2-fold excess concentrations) in the assay mixture

π-Acceptor	Analyte	Another PASH component	ν, cm^{-1}
DDQ	DBT	$DBTO_2$	769, 1045, 1136, 1321, 1477, 1596, 1674
DDQ	4,6-DMDBT	$DBTO_2$	792, 1050, 1176, 1250, 1344, 1569, 1589, 1674
TCNQ	DBTO	$DBTO_2$	1205, 1390, 1455, 1606

Fig. S14 shows that the SERS spectra of DDQ and DDQ with a sample of diesel fuel (Euro-5) are the same, so it can be concluded that the content of DBT and its alkyl derivatives in a sample of diesel fuel is not greater than LOD of 5 ppm, indicating that claimed as a diesel fuel quality. On the spectrum of DDQ with a mixture of model system DBT:4,6-DMDBT:DBTO (1:9:10) in iso-C_8H_{18} formation of CTC are clearly seen since appearance of characteristic signals of DBT and 4,6-DMDBT structural fragments.

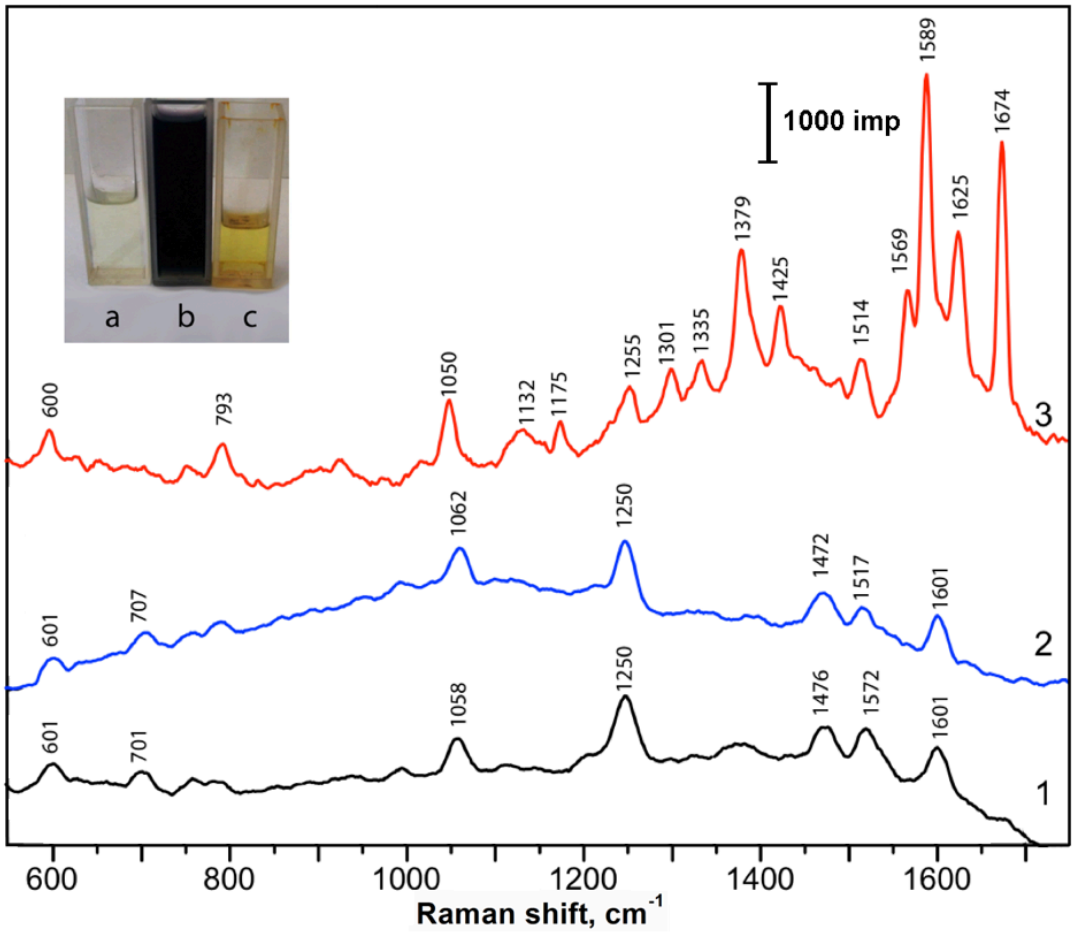

Figure S14. SERS spectra of sensor surface modified with 5 mM DDQ (1), "Euro-5" quality diesel fuel on this surface (2), and 0.01 mM model mixture DBT:4,6-DMDBT:DBTO 1:9:10 in isooctane (3). The inset shows photographs of analyzed diesel fuel (a), 5 mM DDQ in $CHCl_3$ (c), and the mixture of the diesel fuel sample and 5 mM DDQ in $CHCl_3$ (b).

The proposed approach provided novel nanostructures with tunable SERS response and could be applied to the multiplexed analysis (Fig. S15) of PASHs with rather low limits of detection.

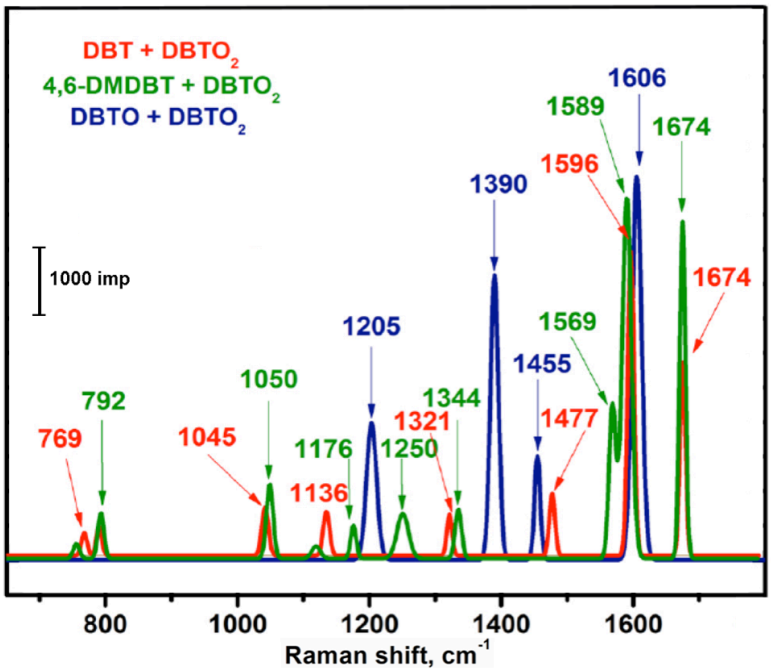

Figure S15. SERS spectra of major sulfur organic markers of oil quality in the presence of a basic conversion product: $DBTO_2$ (sulfone) in the diesel fuel sample and 5 mM DDQ.

It is known that the content of polycyclic aromatic hydrocarbons in diesel fuel is much higher than the content of sulfur-containing aromatic compounds. Diesel fuel contains an average of approximately 75% saturated hydrocarbons (10 – 40% of *n*- and *iso*-alkanes and 20 – 60% cycloalkanes) and 25% PAH (such as alkyl-naphthalenes). Typically, the average formula of diesel fuel is $C_{12}H_{23}$ (average of $C_{10}H_{20}$ to $C_{15}H_{28}$). Various PAHs as discussed above PASHs are also able to serve as π-donors in charge transfer complexes. Therefore, present in the sample solution PAHs, can have a strong depleting effect on the determination of sulfur organic compounds. We studieded the possibility of DDQ/TCNQ to form complexes with 6 model PAH: biphenyl ($C_{12}H_{10}$), naphthalene ($C_{10}H_8$), anthracene ($C_{14}H_{10}$), phenanthrene ($C_{14}H_{10}$), acenaphthene ($C_{10}H_{12}$) and pyrene ($C_{16}H10$) in a solvent system *iso*-C_8H_{18}. These compounds are the main possible oil components causing interferences for the proposed approach (Fig. S16).

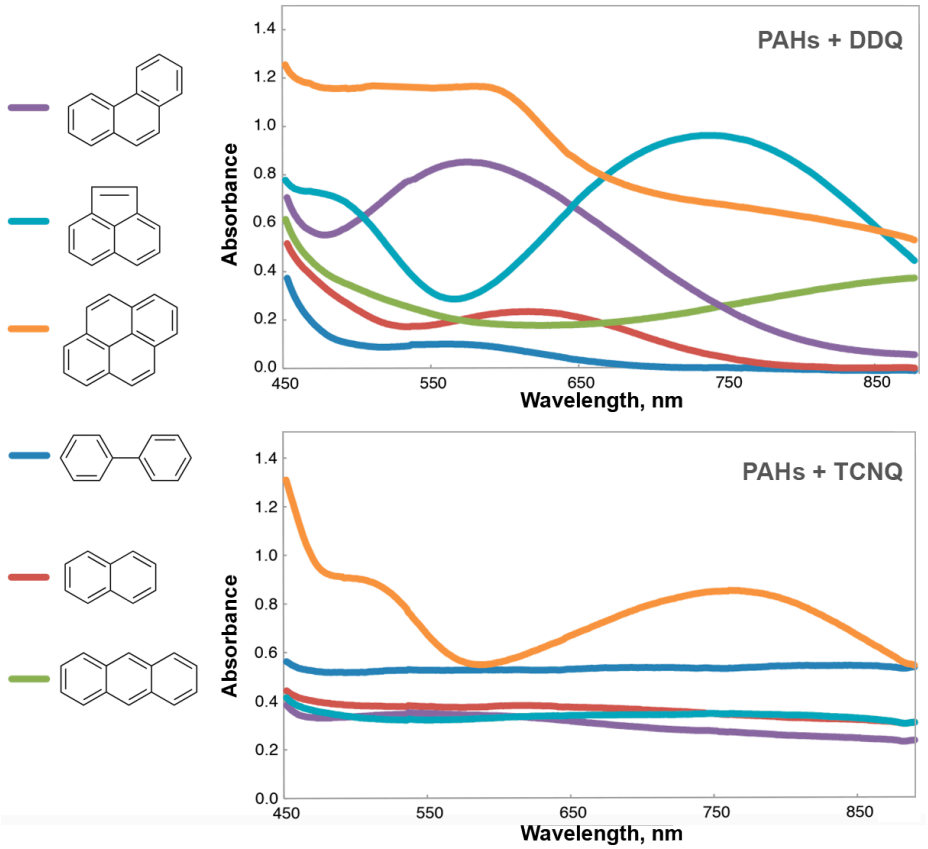

Figure S16. Absorbance spectra of CTCs for PAHs – the main possible oil components causing interferences for the proposed approach.

Figure S17. Photography of SERS-active substrates for diesel fuel analysis.

ABBREVIATIONS

AgNP, silver nanoparticle; ASP, aerosol silver pyrolysis; CTC, charge transfer complex; CS, chitosan; DBT, dibenzothiophene; DBTO, dibenzothiophene sulf-5-oxide; $DBTO_2$, dibenzothiophene sulf-5,5-dioxide; 4,6-DMDBT, 4,6-dimethyldibenzothiophene; DDQ, 2,3-dichloro-5,6-dicyano-1,4-benzoquinone; GC-FID, gas chromatography with flame-ionization detector; GC-MS, mass selective detector; GC-SCD, sulfur chemiluminescence detector; HEC, hydroxyethylcellulose; HPLC-UV, high performance liquid chromatography with UV-detector; PAH, polycyclic aromatic hydrocarbons; PVA, polyvinyl alcohol; PVP, polyvinylpyrrolidone; SERS, surface enhanced Raman scattering; TCNQ, 7,7,8,8-tetracyanoquinodimethane.

REFERENCES

(S1) Foster, R.; Hammick, D. L.; Wardley, A. A. Interaction of Polynitro-Compounds with Aromatic Hydrocarbons And Bases. Part XI. A New Method for Determining the Association Constants for Certain Interactions between Nitro-Compounds and Bases in Solution. J. Chem. Soc. 1953, 3817-3820.